Lasing and squeezing of composite bosons in a semiconductor microcavity

F. Tassone
Quantum Entanglement Project, ICORP, JST, Ginzton Laboratory, Stanford University, Stanford, California 94305 and SISSA-ISAS, via Beirut 2-4, I-34014 Trieste, Italy

Y. Yamamoto
Quantum Entanglement Project, ICORP, JST, Ginzton Laboratory, Stanford University, Stanford, California 94305
(Received 6 January 2000; revised manuscript received 5 May 2000; published 13 November 2000)

We consider a semiconductor microcavity etched into a small post structure in which the polariton modes become quantized. When moderate amounts of excitons are injected, large gain for the lowest confined polariton results from exciton-exciton scattering. We show that gain is sufficient to compensate for typical losses of GaAs structures, and stimulated emission of the confined polariton is eventually achieved at an exciton density below that where Rabi splitting collapses. We study the dependence of the threshold exciton density on post size, polariton loss rate and lattice temperature. We study the polariton statistics, and show that far above threshold, typical transition from super-Poissonian to Poissonian statistics is preserved. Exciton-exciton interaction produces a self-phase modulation, resulting in enhanced frequency noise, and into a net increase of the emission linewidth far above threshold. We show how to produce a number-squeezed state using correlation between frequency and number noise. A numerical example of a realistic structure is also analyzed in detail.

PACS number(s): 42.50.−p, 42.55.Sa, 03.75.Fi, 71.35.Lk

I. INTRODUCTION

The elementary excitation of a semiconductor (exciton) is a bound pair of two fermions, the electron and the hole. It is the analog of the hydrogen atom, and characterized by a binding energy E_B and a Bohr radius a_B. Therefore, it is a composite boson. In particular, when the system is dilute, i.e., when $n_{exc}a_B^2 \ll 1$, where n_{exc} is the excitation density, a bosonic description of the system is convenient. Conceptually, stimulated emission of composite bosons should be realizable, and has been proposed both in the context of thermal equilibrium (condensation) and in the context of nonequilibrium (dynamical condensation or lasing). Renewed interest in this subject followed the realization of two-dimensional polaritons in semiconductor microcavities [1,2]. Polaritons are the mixed modes of a quantum-well (QW) exciton and a cavity photon. Mixing (or strong coupling) is a coherent process where energy is periodically exchanged between a material degree of freedom (exciton) and the electromagnetic mode (cavity photon), characterized by a Rabi oscillation period or equivalently by a Rabi splitting $\hbar\Omega$. Preservation of coherence in the oscillation demands microcavities with high quality factors, showing relatively long photon lifetimes of few ps. Clearly, polaritons are also bosons at low density. Their extremely small mass was suggested to ease their dynamical condensation at low density and relatively large temperatures [3]. We note that stimulated emission of polaritons is conceptually different from that of cavity photons, as polaritons bear a substantial excitonic component. Moreover, this material component is the origin of the gain. Thus, stimulated emission of polaritons is analogous to that of bosonic atoms inside a trap [4]. First attempts to observe stimulated emission of cavity polaritons were unsuccessful [5], because the quasithermalization assumptions cannot be fulfilled at low densities, due to a relaxation bottleneck in the dynamics [6]. Here we show that exciton-exciton scattering at large density provides significant gain for polaritons, and eventually, stimulated emission sets in, when the polariton lifetime is sufficiently long. We further consider an etched microcavity post (Fig. 1 right) in which the polaritons become quantized, in order to isolate the lasing mode, and simplify the analysis of the statistical properties.

In the planar cavity, the cavity photon, the exciton, and polaritons have an in-plane dispersion, labeled by a wave vector k. The cavity photon effective mass, $m_{ph}=E_{cav}/v^2$, with E_{cav} the cavity resonance energy, and v the speed of light in the material, is almost four orders of magnitude smaller than the exciton mass in GaAs. As a consequence, exciton-photon mixing and splitting is relevant for $k < 0.1k_0 = 0.1E_{cav}/\hbar v \sim 3\times 10^5$ cm^{-1}, as shown in Fig. 1(b), by a continuous line, computed for a GaAs cavity. For $k > 0.1k_0$ the lower polariton becomes excitonlike (hereafter simply exciton), and the upper polaritons, photon like. In the micropost here considered, depicted in Fig. 1(a), the in-plane translational symmetry is lifted. The semiconductor and air refraction indexes are largely different and the post efficiently confines the cavity photon in the lateral directions. We will consider posts of square cross section with $D \leqslant 4$ μm, and assume the in-plane $\mathbf{k}$ quantized to $k_x = n_x\pi/D$ and $k_y = n_y\pi/D$, respectively, with integer n_x, n_y. For good photon confinement, the energies of the micropost polariton modes are those of the planar microcavity polaritons at the quantized in-plane momenta (k_x, k_y). The micropost polariton modes are also shown schematically in Fig. 1(b). The polariton energies are discrete, and those with $k < 0.1k_0$ are well separated. On the contrary, quantized exciton energies still form a quasicontinuum, as the exciton mass is much larger. Therefore, the small micropost system is constituted by a large exciton reservoir, and basically one discrete polariton mode at lower energy.

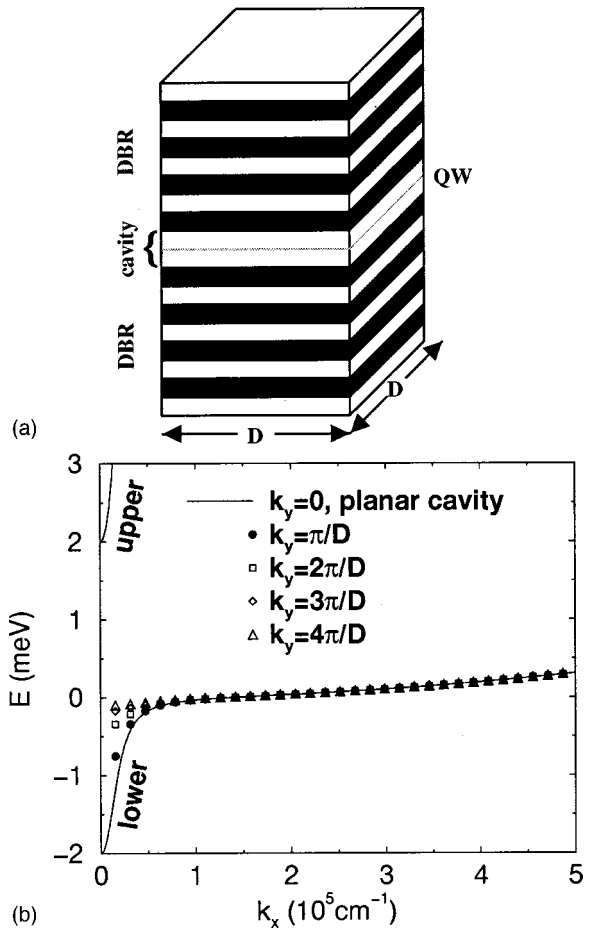

FIG. 1. (a) The micropost structure. The distributed Bragg reflectors are also depicted. (b) The dispersion relation of the microcavity polaritons, in the planar cavity, and the quantized energy/momenta for a $2\mu\text{m}\times 2\mu\text{m}$ post structure. The lowest mode is the confined polariton mode, while other modes, closely packed on the energy axis, form the exciton reservoir.

In this paper, we first study in Sec. II the dynamics of this open system using rate equations that describe gain, spontaneous emission, and recombination for the polariton, and also the dynamics within the exciton reservoir. We calculate in Sec. III the threshold properties of this system. In Sec. IV we extend the rate equations into Langevin equations and calculate noise characteristics of this laser system. We calculate polariton number fluctuations, power and frequency noise spectra, and the emission linewidth. We find that exciton-exciton scattering results in cross- and self-phase-modulation. The former produces an enhancement of the Schawlow-Townes frequency noise spectrum, and the latter a peculiar correlation with number fluctuations. We show that this correlation produces a significant increase of the emission linewidth far above threshold, and that it can be used to completely suppress number fluctuations of the internal polariton field, or to partially suppress number fluctuations in the extracavity photon field by a factor 1/2. A realistic numerical example is also analyzed. Finally in Sec. V we discuss results and their relevance to currently available systems. We also discuss the quantitative and conceptual differences with the bosonic atom laser, and explain what distinguishes polariton lasing from cavity photon lasing.

II. MODEL AND RATE EQUATIONS

Two scattering mechanisms redistribute energy in the system: scattering with phonons and exciton-exciton scattering. Scatterings within the exciton reservoir are much faster than scattering from excitons to the polariton, as quantitatively assessed later. Therefore, excitons are in a quasithermal distribution, whose temperature T_{exc} is fixed by the interplay of heating and cooling processes involving phonon emission and absorption. We could well describe the reservoir and its dynamics with two macroscopic numbers only, an exciton density and an exciton temperature. However, it is easier to model the intrareservoir dynamics and the reservoir-polariton dynamics together within a common framework. We describe the dynamics of populations with rate equations, in which scattering rates are calculated within a Markov approximation (Fermi golden rule). The resulting equations are commonly named quantum Boltzmann equations because final-state stimulation is also included. Validity of this approach has been discussed at length in Ref. [7] and will not be repeated here. Further concerns regarding the application of the Markov approximation to this laser system will be addressed in Sec. IV. Here we only note that we completely ignore renormalization of excitation energies, and in particular, collapse of the Rabi splitting. At large exciton densities n_{exc}, dephasing related to exciton-exciton scattering is large enough to destroy exciton-photon coherence. Eventually at even larger densities, the concept of exciton as a boson becomes meaningless (Mott density). Collapse of the Rabi splitting has been observed in various experimental conditions, and estimated to occur at a density of carriers of 4×10^{10} cm^{-2} in GaAs samples, [8–10] which coincides with our estimate based on exciton-exciton collision rates. In the following, we restrict our analysis to $n_{exc}<4\times 10^{10}$ cm^{-2}. As the collapse of the Rabi splitting is rather abrupt, we expect our results to hold at least qualitatively also close to this limit.

For computational purposes, we discretize the continuous exciton reservoir, using an uniform energy grid $E_i=i\Delta E$, $i=1,2,\ldots$, which is convenient for the flat exciton density-of-states (DOS). We use N_i to label the exciton population $N_i=N(E_i)$. We use the index $i=0$ as a special label for the polariton throughout this paper, with $E_0<0$ the polariton energy. The rate equations read:

$$\dot{N}_i=P_i-\Gamma_i N_i-\sum_{i'}\{W_{i\to i'}N_i(N_{i'}+1)-W_{i'\to i}N_{i'}(N_i+1)\}$$
$$-\sum_{i_1,i',i'_1}\{Y_{ii_1\to i'i'_1}N_iN_{i_1}(N_{i'}+1)(N_{i'_1}+1)$$
$$-Y_{i'i'_1\to ii_1}N_{i'}N_{i'_1}(N_i+1)(N_{i_1}+1)\}. \quad (1)$$

Here P_i is the pump rate, Γ_i the radiative recombination rates plus other losses, $W_{i\to i'}$ the scattering rate with the phonons, and $Y_{ii_1\to i'i'_1}$ the exciton-exciton scattering rates.

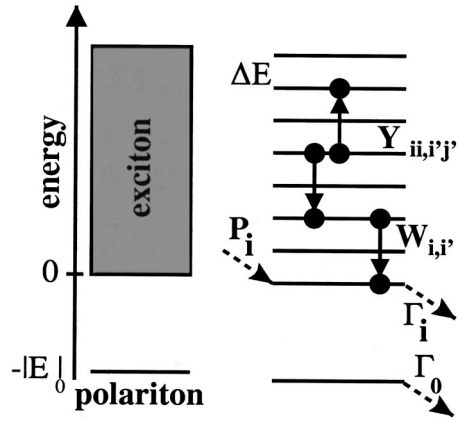

FIG. 2. Left, schematic representation of the microcavity post system, with the exciton reservoir shaded and the single polariton level. Right, the discretized reservoir and schematics of all pumping, decay, and scattering processes included in Eq. (1).

This process conserves energy. A schematic picture of the system and the typical scattering processes is depicted in Fig. 2.

Rate Eq. (1) includes both the spontaneous and the stimulated processes. Indeed, stimulated scattering to the polariton mode and its inverse process—scattering from the polariton to the exciton reservoir—describes the gain and loss processes, respectively, in the traditional laser terminology, as explicitly shown in the Appendix. The expressions and calculation of the various scattering rates in the planar microcavity have been reported in detail in Refs. [6,7]. We only remark that scattering rates within the exciton reservoir are not significantly changed with respect to the planar case. In particular, we may still use conservation of momentum for scattering among the excitons, as they have a thermal wavelength much smaller than the post size. In other words, the thermal distribution of excitons spans a large number of the closely spaced confined states. For the same reason we may assume the polariton modes to have zero momentum when calculating the scattering matrix elements. In order to calculate scattering to and from the confined polariton, we use the same expressions for the planar case given in Ref. [7], in which a fictitious polariton DOS, $\partial E(k)/\partial k^2 = \Delta E S/(4\pi)$, $S=D^2$ the post surface, is introduced. It can be shown that this is exact for the lowest confined mode, having $k_x = k_y = \pi/D$.

We discuss some properties of the processes described in the rate Eq. (1). The exciton-phonon scattering strength can be characterized by the phonon absorption rate of $\mathbf{k}=0$ excitons, which is linear in temperature with a coefficient $\gamma = 5\mu$ eV/K for a typical GaAs QW, 100 Å wide [11], and by a relaxation rate of hot excitons at T=0, of the order of tens of ps [12]. Typical scattering matrix elements span a range $(i-i')\Delta E$ of about 1 meV, depending on the QW width. In the planar cavity, relaxation of excitons into polaritons at $E<0$ is suppressed because of the small polariton DOS [13,6], bringing these relaxation times well above a ns. For the small micropost case, the finite confinement energy and a larger effective polariton DOS results into faster relaxation times, typically in the range of hundreds of ps for the structures considered in this paper.

Exciton-exciton scattering can be characterized by an outscattering rate from $\mathbf{k}=0$ excitons, which is largely independent of T_{exc}, and linearly dependent on the exciton density n_{exc}. For typical GaAs parameters, the rate $\hbar\Gamma_{\mathrm{exc-exc}} \sim (\pi^2 E_B^2/2E_L)(n_{exc}a_B^2) \sim 1$ meV when $n_{exc}=10^{10}$ cm^{-2}. Here $E_L=\hbar^2/m_{exc}a_B^2$. The same values were also independently calculated in Ref. [14]. Experimentally, this rate has been measured with four-wave mixing experiments [15], and by direct measurement of the absorption linewidth [16]. Recently, this rate has been directly measured in microcavities by upper polariton emission [17,18]. While absorption measurements and the microcavity experiment give consistent numbers with theory, Honold *et al.* measured smaller scattering rates by a factor of 5. Discrepancies can be traced back to difficulties in a precise measurement of n_{exc}. The exciton-exciton scattering matrix element is relatively flat in k space for $k<a_B^{-1}$, or as a function of energy within an energy span E_L. As $E_L \gg k_B T$ throughout this paper, we neglect these details. Relaxation of reservoir excitons into polaritons through exciton-exciton scattering is not suppressed as it is for the phonon emission process. This relaxation takes place through scattering of two excitons into a polariton and a hotter exciton: the final DOS for this scattering process is the exciton DOS, and not the much smaller polariton DOS, as it is for phonon scattering. An approximate estimate of this scattering rate is useful and straightforward. The final polariton has an energy $-|E_0|$ and zero momentum, thus, at least an energy $|E_0|$ is released in the scattering to the excitonic reservoir. Considering thermal excitons, the optimal initial condition gives two excitons of energy $|E_0|/2$, and using the Boltzmann distribution, we find a typical scattering rate of $\Gamma_{exc-exc}e^{-|E_0|/k_BT}$, apart from Hopfield factors of order unity. Therefore, this relaxation rate is in the range of few $(\mathrm{ps})^{-1}$ for $k_BT \sim |E_0|$ already at moderate n_{exc}. As this relaxation is a gain process for the polariton, we understand that relevant recombination losses can be compensated at moderate n_{exc}. The inverse processes of scattering of the polariton to other states also effectively contribute to polariton loss. These processes are of course also included in Eqs. (1), and we usually speak of net gain as the difference of gain and these losses, excluding recombination. In planar cavities, scattering out of $\mathbf{k}=0$ polaritons to other polaritons, is largely suppressed by the low final DOS. In the micropost, it is instead trivially suppressed by confinement. On the contrary, scattering to excitons has a relevant final DOS. However, this channel is cutoff at low lattice and exciton temperatures, $k_BT<\Omega/2$ (or $k_BT<|E_0|$ in the post case). This sets an upper bound for temperatures at which any gain mechanism is relevant, and is essentially a material property related to Ω. In particular, net gain resulting from exciton-exciton scattering at a given n_{exc} is small both at low T, where gain is small, and at large T, when loss is large. Thus, an optimal operation temperature $k_BT \sim \hbar\Omega$ exists.

The radiative recombination rates Γ_i in principle depend on the structure of the post, but to lowest order they can be calculated from the planar cavity case, as for the dispersion. For the lowest confined mode, lateral (post) confinement re-

sults in $|E_0|<\hbar\Omega/2$, and a reduced photon content. The resulting radiative lifetime $\tau_0=\Gamma_0^{-1}$ is expected to be longer than twice the cavity photon lifetime. In particular, in the structures considered, photon lifetime is $\sim$1 ps, and the calculated confined polariton lifetime exceeds 10 ps. This is still a very short lifetime. Presumably, other loss processes—finite leakage through the side walls due to surface roughness, and nonradiative exciton recombination introduced by the etching process—do not lower it significantly. However, in view of the realization of better cavities showing longer photon lifetimes in the near future, in place of the calculated recombination rate, we use an effective polariton loss rate in a range of reasonable values, 10 ps–100 ps. As for the radiative lifetime of excitons $\Gamma_{i>0}$, related to the leaky modes of the dielectric mirrors, [19] we use the calculated values. Slightly modified structure of the leaky modes due to lateral confinement does not drastically change any result presented in this paper, and in particular, the exciton density at threshold.

III. THRESHOLD BEHAVIOR

In this section we present numerical results from the integration of the rate Eq. (1) in stationary conditions, $d/dt=0$. We model an optical pump injecting cold excitons close to $E=0$, having a Gaussian distribution in energy $P_i \propto e^{-E_i^2/\sigma^2}P$, with $\sigma=0.25$ meV. We also use $\Delta E=0.1$ meV. Choice of this parameter is discussed in detail in Ref. [7]. In stationary conditions we find that the excitons thermalize to a temperature T_{exc}, which is close to the lattice temperature T. We first consider $D=2$ μm. The polariton has an energy $E_0=-0.7$ meV, as shown in Fig. 1. We fix the recombination rate of the confined polariton to $\tau_0=\Gamma_0^{-1}=10$ ps.

We plot in Fig. 3(a) the population of the confined polariton and the exciton density on a double-logarithmic scale and (b) T_{exc} as a function of the pump intensity, and for three different lattice temperatures T. As expected, we notice a clear threshold behavior in the population, and clamping of the exciton density when stimulated emission sets in. In the double-logarithmic plot of Fig. 3(a) the threshold clearly appears at a population of $N_0=1$ (later adopted as a definition of threshold), proving its origin in stimulated emission. We notice that clamping of the exciton density is moderate, and that a sizeable heating of excitons appears above threshold, especially for $T=2$ K. A hysteresis is also found for $T=2$ K, which is related to an abrupt change of T_{exc} as stimulated emission sets in. The hysteresis is related to the pumping efficiency: the average exciton radiative lifetime $\tau_{exc}=(\Sigma\Gamma_i N_i/\Sigma N_i)^{-1}$ is in fact linearly dependent on T_{exc}, as only excitons of small wave vector $k<k_0$ radiatively recombine [20]. For $T=2$ K, T_{exc} doubles across threshold, Fig. 3(b), and so does τ_{exc}. The exciton pumping efficiency also doubles, as below or around threshold it is proportional to $P\tau_{exc}$. This positive feedback makes the system unstable, and results in hysteresis. Experimentally, $\tau_{exc}\propto T_{exc}$ is observed only for $T_{exc}>10$ K. Both nonequilibrium [12] and exciton localization [21] effects contribute to a flattening of this dependence at low temperature. Localization effects are clearly not accounted for in our approach, and we thus expect observation of hysteresis in highest quality samples only.

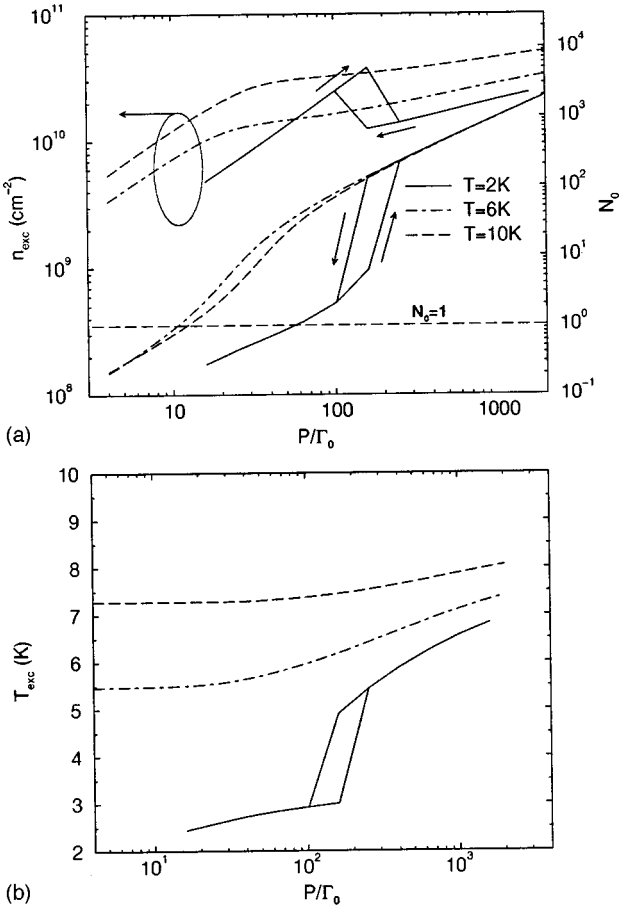

FIG. 3. (a) Exciton density, left, and polariton population, right, and (b) exciton temperature T_{exc} vs pump intensity for three different temperatures. $\tau_0=10$ ps and a 2×2 μm post structure was considered. Other parameters are given in the text.

Clearly, exciton heating proves that exciton-exciton scattering is the basis of gain. Indeed, we remarked before that at least an energy $|E_0|$ is released to the reservoir for every exciton scattering into the polariton. The reservoir dissipates the excess energy only through phonon emission events: a given T_{exc} results from the balance between in-flow and outflow energy rates. Phonon absorption and emission rates are balanced when $T_{exc}=T$, and energy dissipation is roughly proportional to $(T_{exc}-T)$. The net inflow from the gain process is instead proportional to N_0, thus $(T_{exc}-T)\propto N_0$. Heating of the reservoir is an essential aspect of gain resulting from exciton-exciton collisions, and its experimental observation would provide a strong evidence for this origin. We finally remark that increase of T_{exc} above threshold decreases exciton-exciton scattering efficiency as explained in Sec. II, and results in incomplete clamping of n_{exc}.

We plot in Fig. 4 the exciton density at threshold as a function of T, using otherwise the same parameters as before. We note that the lowest threshold is obtained for $k_BT=0.3$ meV, which is of the order of $|E_0|=0.7$ meV, as expected. In Fig. 5 we report the dependence of n_{exc} at threshold, for T

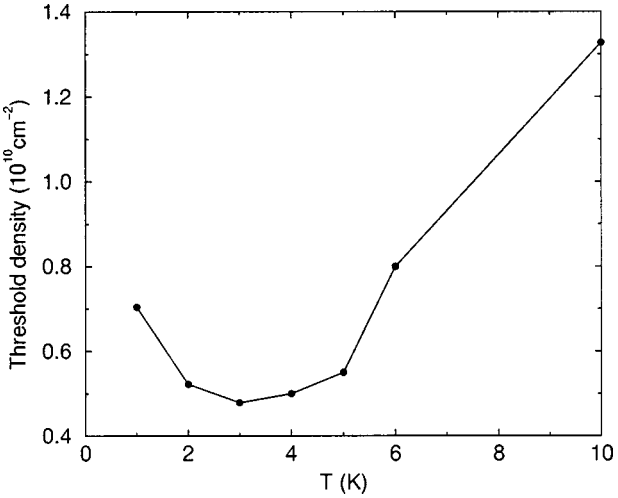

FIG. 4. Exciton density at threshold vs the lattice temperature, for $\tau_0=10$ ps and a 2×2 μm post structure. Other parameters are given in the text.

$=6$ K, as a function of τ_0, for both $D=2$ μm and $D=4$ μm. As expected, n_{exc} is a decreasing function of τ_0. The threshold density shows an asymptotic value for $\tau_0\to\infty$, which is close for both post sizes.

In order to simplify the analysis of threshold, we neglect the difference between T and T_{exc} and bosonic degeneracy in the reservoir, and retain only the rate equation for the polariton mode:

$$\frac{dN_0}{dt}=R_{in}(1+N_0)-R_{out}N_0=R_{sp}+GN_0. \tag{2}$$

Here R_{sp} and G are the spontaneous emission and net gain. We define $N_{exc}=n_{exc}\lambda_{th}^2$, where $\lambda_{th}^2=2\pi\hbar^2/m_{exc}k_BT$ is the squared thermal wavelength of excitons. The rates are then given by

$$R_{in}=\Gamma'_{ph}N_{exc}+\Gamma'_{e-e}N_{exc}^2, \tag{3}$$

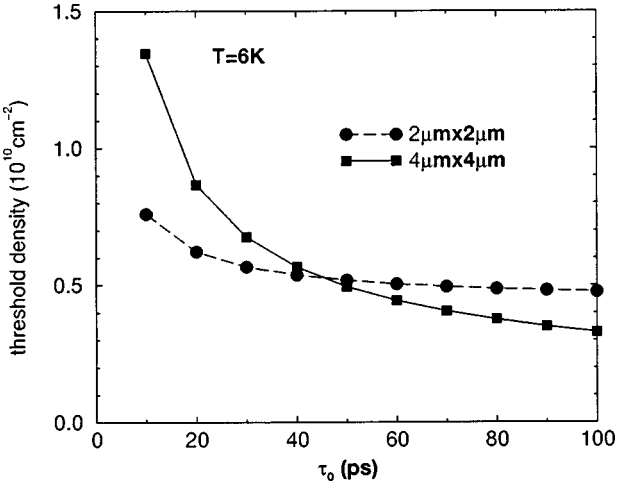

FIG. 5. Exciton density at threshold vs the total polariton lifetime, for two different post structures. Other parameters for this Group-III–V system are given in the text.

$$R_{out}=\Gamma_0+\Gamma_{ph}+\Gamma_{e-e}N_{exc}. \tag{4}$$

Here Γ_{ph},Γ'_{ph} are total phonon absorption and emission rates, and $\Gamma_{e-e},\Gamma'_{e-e}$ the exciton-exciton collision rates. Thermal equilibrium within the reservoir imposes the detailed balance of all scattering processes:

$$\Gamma_{ph}=e^{-\beta|E_0|}\Gamma'_{ph},\quad \Gamma_{e-e}=e^{-\beta|E_0|}\Gamma'_{e-e}. \tag{5}$$

Here $\beta=1/(k_BT_{exc})$. At threshold, $N_0=1$, then Eq. (2) may be solved for N_{exc} in stationary conditions. When also $\Gamma_{e-e}\gg\Gamma'_{ph}$

$$N_{exc}=\frac{\Gamma_{e-e}+\sqrt{\Gamma_{e-e}^2+8\Gamma'_{e-e}\Gamma_0}}{4\Gamma'_{e-e}}. \tag{6}$$

It shows a minimum threshold density $N_{exc}=1/2\exp(-\beta|E_0|)$ when $\Gamma_0\ll\Gamma_{e-e}$. This is clearly the thermal equilibrium condition between the polariton and excitons, with a chemical potential $\mu\sim-|E_0|$. The calculated asymptotic density at T=6 K is $n_{exc}=5.5\times10^9$ cm^{-2}, while that fitted from the results in Fig. 5 is $n_{exc}=4.5\times10^9$ cm^{-2}, showing good agreement. The fit also gives $\Gamma_{e-e}=3.0\times10^{11}$ s^{-1} for $D=2$ μm. It should also be noted that the very same functional form for the threshold density Eq. (6) is obtained when $\Gamma_{ph}\gg\Gamma_{e-e}$. Therefore, heating effects are a clear and unique fingerprint of exciton-exciton scattering as the origin of gain. We have also numerically separated the two contributions to gain, for $D=2$ μm, T=6 K, and found $\Gamma'_{e-e}\sim3\Gamma'_{ph}$. The rate Γ'_{ph} is somewhat larger than in planar microcavities because of polariton confinement. Moreover, we note it is a rapidly decreasing function of the QW width (here we used 100 Å), as described in detail in Ref. [7], whereas exciton-exciton scattering has a weaker dependence on it through the exciton binding energy.

The maximum gain that can be expected from exciton-exciton scattering in a given material may be roughly estimated using the results of Ref. [7]:

$$\hbar\Gamma'_{e-e}=\pi^3|X|^2\frac{E_B^2}{k_BT}\frac{a_B^4}{\lambda_{th}^4}e^{-\beta|E_0|}. \tag{7}$$

Here $|X|^2$ is the exciton content of the polariton mode, the exciton thermal wavelength λ_{th} has been introduced before, as well as the other quantities. Using $k_BT\sim|E_0|$, close to the optimal value, gain becomes proportional to $n_{exc}^2E_B^2/|E_0|$. The maximum allowed $n_{exc,max}$ is found at Rabi splitting collapse, and given by the condition $\hbar\Gamma_{exc-exc}\sim\hbar\Omega$. Then, $n_{exc,max}\propto\hbar\Omega E_L/E_B^2$, with E_L introduced before. Thus, the maximum gain is

$$G_{max}\propto\hbar^2\Omega^2E_L^2/(E_B^2|E_0|).$$

For planar cavities at zero detuning, we use $|E_0|=\hbar\Omega/2$ and $G_{max}\propto\hbar\Omega E_L^2/E_B^2$. In Group-II–VI materials such as ZnSe, G_{max} is expected to be significantly larger than in GaAs, as E_L/E_B is similar, but $\hbar\Omega$ is significantly larger. With respect to the planar case, lasing in the micropost structure has the

additional advantage of having $|E_0|<\hbar\Omega/2$, and longer polariton lifetimes as remarked before. Of course, these same advantages can be obtained in planar cavities using positive detuning. However, in practice $|E_0|$ cannot be made too small: well before the lowest polariton mode of a planar microcavity becomes significantly massive, additional loss mechanisms beside radiative recombination can be expected, such as elastic scattering from the lowest polariton states to localized exciton states.

IV. LANGEVIN EQUATIONS AND NOISE PROPERTIES

Noise properties of polariton lasing process are related to quantum-mechanical fluctuations of the occupation of the state around its average value. Therefore, we need to describe the quantum-mechanical evolution of the polariton state coupled to external reservoirs, beyond rate Eq. (1), in which only the average occupation is calculated. A convenient description of this quantum-mechanical evolution is given by Langevin equations [22]. In deriving them, we treat the exciton reservoir as ideal, and neglect any phase coherence in it. We assume that exciton phases are instantaneously washed out by fast scattering processes within the reservoir. This assumption needs further discussion, as it is central to further developments of the theory of bosonic lasers. Eventually far above threshold, when $N_0 \gg 1$, this assumption does not hold anymore because of stimulated scattering. Then, the nature of the exciton states changes. In the equilibrium theory of the interacting Bose gas, it is well known that when the macroscopic condensate forms, strong interaction between the condensate and bosons at long wavelength (small wave vector) renormalizes them into phononlike quasi-particles. Technically, these new states are found with a diagonalization of the strongest interaction terms, with a Bogolyubov transformation [23]. If we call $\mathcal{W}\sim 6E_B a_B^2/S$ the effective interaction between bosons [7], modes up to an energy $\mathcal{W}|\mathcal{A}|^2/2$ are renormalized into phononlike quasiparticles. Here $\mathcal{A}$ is the condensate amplitude, then $N_0 = |\mathcal{A}|^2$. Therefore, we may safely neglect renormalization effects when $\mathcal{W}N_0/2<|E_0|$. For $D=2$ μm we obtain $N_0 < 1.5\times 10^3$, and four times as much in the larger $D=4$ μm post case. Qualitatively, renormalization of low-energy excitons into phononlike modes results in a decrease of exciton-exciton scattering, and therefore also gain. This adds onto the usual saturation due to population depletion [7]. The resulting slow down of the relaxation dynamics in the reservoir is accompanied by larger fluctuations in the reservoir, and possibly a qualitative change in the noise properties of the system. In the following, we neglect all these effects, and consider results with $N_0>1.5\times 10^3$ as indicative only. Saturation effects are instead fully addressed. We also neglect deviations of the exciton population distribution from the thermal one, assuming that also these fluctuations are instantaneously washed out. In principle we could take into account temperature fluctuations, but we expect these to have a minor effect, and do not include them. Changes of the average T_{exc} are instead included and will be discussed later.

In the Appendix A we directly calculate the drift and noise terms generated by exciton-exciton scattering up to second order in $\mathcal{W}$. Here we note that the real parts of the drift terms could also have been directly read off from the rate equations, as these are derived within the same assumptions (Markov approximation, unperturbed nature of the exciton states, and scattering to second order in $\mathcal{W}$), and we are dealing with a bosonic system. The corresponding noise terms easily follow. Instead, the imaginary part of the drift terms (frequency shifts) do not appear in the rate equations, and have to be calculated microscopically (see Appendix A). We also note that real and imaginary parts of the drift terms obey the causality principle and are related by a Kramers-Krönig transformation. Consistently with the above assumptions on the exciton reservoir dynamics, we do not need to consider each individual $N_{\mathbf{k}}=b_{\mathbf{k}}^\dagger b_{\mathbf{k}}$, where $b_{\mathbf{k}}$ is the exciton destruction operator, as an independent dynamical variable, and the Langevin equations finally read:

$$\dot{B}_0=\frac{G-\Gamma_0}{2}B_0-i\left[\frac{\mathcal{W}}{2}|X_0|^4N_0+\epsilon(N)\right]B_0+F_{B_0}+F_{\Gamma_0}, \tag{8}$$

$$\dot{N}=p-\Gamma N-GN_0-R_{sp}+F_\Gamma+F_p+F_N. \tag{9}$$

Here B_0 is the destruction operator for the polariton mode, in the rotating frame (see Appendix A), $N_0=B_0^\dagger B_0$, $N=\Sigma_{\mathbf{k}}N_{\mathbf{k}}$ is the total number of excitons, and $p\propto P$ is the total pumping rate. The gain G is the net gain, i.e., it includes scattering out terms, and is written as

$$G=\zeta^2\Gamma'_{e-e}N^2+\zeta\Gamma'_{ph}N-\zeta\Gamma_{e-e}N-\Gamma_{ph}, \tag{10}$$

whereas the spontaneous emission terms are

$$R_{sp}=\zeta^2\Gamma'_{e-e}N^2+\zeta\Gamma'_{ph}N. \tag{11}$$

$\zeta=\lambda_{th}^2/S$ and the scattering rates were introduced in Sec. III. Γ is the average of the exciton recombination rate Γ_i over a thermal distribution. The imaginary terms in Eq. (8) are the self-energy shifts up to second order in $\mathcal{W}$. In particular, $\epsilon(N)$ is the polariton-energy modulation by change of carrier density, analogous to that in conventional lasers, where modulation of the carrier density results in a change of the index of refraction, and a change of the lasing frequency. The $|X_0|^4\mathcal{W}N_0/2$ term is instead unique to this system, as it is generated by the microscopic Hamiltonian term $\hbar\mathcal{W}|X_0|^4b_0^\dagger b_0^\dagger b_0 b_0/4$. Such an interaction is missing in the conventional photon laser, where the mode b_0 is a photon. This type of interaction is also found for photons propagating in a Kerr medium [22]. The effect of this interaction is to modulate the phase of the lasing mode, and therefore has been named self-phase modulation. A phase-number correlation results from this self-phase modulation, which was also discussed for light passing through a Kerr medium in Ref. [24].

The noise sources $F(t)$ in Eq. (8) are approximated with white-noise sources, so as to preserve the commutation relation of B_0. They originate in the coupling to the exciton and the external photon reservoirs, respectively, and have the following statistical properties:

$$\langle F^{\dagger}_{B_0}(t)F_{B_0}(t')\rangle = \langle R_{sp}\rangle \delta(t-t'), \tag{12}$$

$$\langle F_{B_0}(t)F^{\dagger}_{B_0}(t')\rangle = \langle R_{sp}-G\rangle \delta(t-t'), \tag{13}$$

$$\langle F^{\dagger}_{\Gamma_0}(t)F_{\Gamma_0}(t')\rangle = 0, \tag{14}$$

$$\langle F_{\Gamma_0}(t)F^{\dagger}_{\Gamma_0}(t')\rangle = \Gamma_0 \delta(t-t'). \tag{15}$$

The other noise sources in Eq. (9) are also approximated with white-noise sources, and are related to the radiative decay process, the pump process, and exciton-exciton scattering processes, respectively. They have the following properties:

$$\langle F_p(t)F_p(t')\rangle = p\,\delta(t-t'), \tag{16}$$

$$\langle F_N(t)F_N(t')\rangle = [\langle R_{sp}-G\rangle\langle N_0\rangle + \langle R_{sp}\rangle(1+\langle N_0\rangle)] \times \delta(t-t'), \tag{17}$$

$$\langle F_\Gamma(t)F_\Gamma(t')\rangle = \Gamma\langle N\rangle \delta(t-t'). \tag{18}$$

These last sources do not have cross correlations, and also with the previous one in Eq. (14). Instead the real part of F_{B_0} is correlated to F_N as they both originate from the same interaction Hamiltonian. In particular, the operator $N+N_0$ commutes with the exciton-exciton interaction Hamiltonian, as this interaction conserves the number of bosons. When the Langevin equation for $\dot{N}_0$ is derived from Eq. (8), the drift terms originating from exciton-exciton scattering are exactly opposite to those in Eq. (9). Therefore, $F_N + F_{N_0} = 0$ exactly, and

$$\langle F_{N_0}F_{N_0}\rangle = \langle F_N F_N\rangle = -\langle F_N F_{N_0}\rangle. \tag{19}$$

We also note that in the Langevin Eq. (8), N, G, and R_{sp} are operators.

The Langevin equations written above are similar to those of a conventional laser [25,26] with the exception of the different gain mechanism, and the new self-phase modulation term. As customary in laser theory, the above equations are studied below or about threshold, when $\langle N_0\rangle \sim 1$, and very much above threshold, when $\langle N_0\rangle \gg 1$. In the first case, we neglect the coupling of fluctuations of N to N_0 as the fluctuations are small, and substitute for G its average $\overline{G} = \langle G\rangle$. Number fluctuations are easily derived from

$$\dot{N}_0 = (\overline{G}-\Gamma_0)N_0 + \overline{R}_{sp} + F_{N_0}, \tag{20}$$

and result in super-Poissonian noise near the threshold. Far above threshold, we introduce Hermitian amplitude and phase operators, δB_0 and ϕ, respectively, by

$$B_0 \equiv (\overline{B}_0 + \delta B_0)e^{-i\phi},$$

with $\overline{B}_0 = (\langle B_0 + B_0^{\dagger}\rangle)/2$. We also introduce $N = \overline{N} + \delta N$ and $\delta N_0 = 2\overline{B}_0 \delta B_0$. We obtain to lowest order in $\delta N_0, \delta N$

$$\dot{\phi} = \frac{i}{2\overline{B}_0}[F_{B_0} - F_{B_0^{\dagger}} + F_{\Gamma_0} - F^{\dagger}_{\Gamma_0}] + \frac{3|X_0|^4}{4}\mathcal{W}\delta N_0 + \frac{d\epsilon(\overline{N})}{d\overline{N}}\delta N + \epsilon(\overline{N})\frac{\delta N_0}{2\overline{N}_0}, \tag{21}$$

$$\dot{\delta N}_0 = (\overline{G}-\Gamma_0)\delta N_0 + \eta\,\delta N + F_{N_0} + F'_{\Gamma_0}, \tag{22}$$

$$\dot{\delta N} = -\overline{G}\,\delta N_0 - (\Gamma + \eta + \eta')\delta N + F_\Gamma + F_p + F_N. \tag{23}$$

Here $\eta = \overline{N}_0 d\overline{G}/d\overline{N}$, $\eta' = d\overline{R}_{sp}/d\overline{N}$, and $F'_{\Gamma_0} = \overline{B}_0[F_{\Gamma_0} + F^{\dagger}_{\Gamma_0}]/2$. We note that we neglect the average energy-level shifts, which appear in the phase equations and typically amount to fractions of a meV in the considered cases. These average shifts represent a change of lasing frequency with carrier density, and are part of the renormalization effects discussed before. We also neglected phase operators in the number equations, as the phase is slowly fluctuating and decouples from the faster number fluctuations, far above threshold. The self-phase modulation term is $3/4\times|X_0|^4\mathcal{W}\delta N_0$. The other terms $(d\epsilon/d\overline{N})\delta N$ and $\epsilon(\overline{N})\delta N_0/2\overline{N}_0$ are conventional amplitude to phase coupling terms.

A. Number fluctuation and Poisson limit

Equations (22) and (23) are solved by standard Fourier-transform techniques, and the power spectra are calculated taking into account the auto and cross correlations of the noise sources. We define the Fourier transform of an operator as

$$\tilde{F}(\omega) = \lim_{T\to\infty}\sqrt{\frac{2}{T}}\int_{-T/2}^{T/2} dt\, e^{i\omega t}F(t).$$

We Fourier transform Eqs. (22) and (23) and obtain the linear system:

$$\begin{aligned}(\Gamma_0 - \overline{G} + i\omega)\tilde{\delta N}_0 - \eta\tilde{\delta N} &= \tilde{F}_{N_0} + \tilde{F}'_{\Gamma_0}\\ \overline{G}\tilde{\delta N}_0 + (i\omega + \Gamma + \eta + \eta')\tilde{\delta N} &= \tilde{F}_\Gamma + \tilde{F}_p + \tilde{F}_N.\end{aligned} \tag{24}$$

The solutions are explicitly worked out in Appendix B, where also the noise power spectra are calculated.

Here, we consider the limit case of the system very far above threshold, defined as $\overline{N}_0 \gg \overline{N}$. Then, $\overline{G}\sim\Gamma_0$ and $\eta \gg \Gamma_0, \Gamma, \eta'$, as $\eta \propto \overline{N}_0$. The Fourier transform of δN_0 reads, with $\omega < \eta$:

$$\tilde{\delta N}_0(\omega) \sim \frac{\tilde{F}_N + \tilde{F}_{N_0} + \tilde{F}'_{\Gamma_0} + \tilde{F}_p + \tilde{F}_\Gamma}{i\omega + \Gamma_0}. \tag{25}$$

The power spectrum of $\tilde{\delta N}_0(\omega)$ is clearly Lorentzian of width Γ_0. We recall that $F_N + F_{N_0} = 0$ from Eq. (19), and we are left with the noise contributions of the pump and recombination processes only. Eventually, the noise contribution

from F_Γ becomes also negligible when $\Gamma\bar{N}\ll\Gamma_0\bar{N}_0$. Then, the total noise power $\langle\delta N_0^2\rangle\sim\bar{N}_0$, and the usual Poissonian fluctuations are recovered. In this limit, the autocorrelation of δN becomes also Lorentzian, of width η, and total power $\bar{N}_0\bar{R}_{sp}/\eta$. The cross correlation of δN and δN_0 has two Lorentzian contributions, one of width η, the other of width Γ_0, the first contributing a total noise power $-(2\bar{R}_{sp}-\Gamma_0)\bar{N}_0/\eta$, the second $-\bar{N}_0\Gamma_0/\eta$.

As an example, we consider the $D=2$ μm micropost, at $T=6$ K. From Fig. 3, we read $n_{exc}=2\times10^{10}$ cm^{-2}, and deduce $\bar{N}\sim800$ above threshold. Clamping of the reservoir number is far from ideal, due to exciton heating effects. Also when $\bar{N}_0>800$, the Rabi splitting collapses. Therefore, in this structure it is not possible to reach the far-above-threshold regime. The situation is only slightly better for $T=3$ K, where the threshold density is almost halved. Still, we calculated that $\bar{N}_0\sim\bar{N}$ when Rabi splitting collapses, because of exciton heating effects. We report in Fig. 6 the total noise power as a function of $\bar{N}_0$. We note that the total noise power for N_0 is significantly smaller than super-Poissonian $\bar{N}_0(\bar{N}_0+1)$, related to stimulated emission, yet the Poissonian limit is still not attained even at the largest $\bar{N}_0$ allowed.

B. Polariton squeezing

We next calculate the frequency noise spectrum, which easily follows from Eq. (21). We obtain

$$\begin{aligned}P_{\dot\phi^\dagger\dot\phi}=&\frac{2\bar{R}_{sp}-\bar{G}+\Gamma_0}{4\bar{N}_0}+\left(\frac{3}{4}\mathcal{W}|X|^4+\frac{\epsilon(\bar{N})}{2\bar{N}_0}\right)^2\\&\times P_{\delta N_0^\dagger\delta N_0}+\left(\frac{d\epsilon}{d\bar{N}}\right)^2P_{\delta N^\dagger\delta N}\\&+\frac{d\epsilon}{d\bar{N}}\left(\frac{3}{4}\mathcal{W}|X|^4+\frac{\epsilon(\bar{N})}{2\bar{N}_0}\right)\\&\times P_{\delta N^\dagger\delta N_0+\delta N_0^\dagger\delta N}.\end{aligned}\tag{26}$$

The power noise spectra are explicitly given in Eqs. (B3)–(B5). The first term in Eq. (26) is the usual phase diffusion resulting from the spontaneous emission, which gives rise to the Schawlow-Townes linewidth of the laser. We recall that the $3\mathcal{W}|X_0|^4/4$ is the self-phase modulation contributions, while the other contributions originate from the usual phase modulation through the carrier population. We noted above, that far above threshold, the fluctuations of N_0 dominate over those of N. In this case, the self-phase modulation dominates over the other phase-diffusion mechanisms discussed before. Then, we may write

$$P_{\dot\phi^\dagger\dot\phi}(\omega)\sim\left(\frac{3}{4}\mathcal{W}|X|^4\right)^2P_{\delta N_0^\dagger\delta N_0}(\omega).$$

At low frequency, $\omega<\Gamma_0$, $P_{\delta N_0^\dagger\delta N_0}(\omega)\sim4\bar{N}_0/\Gamma_0$. We show that this strong phase noise can be used to reduce the polariton number fluctuations. We consider a new operator:

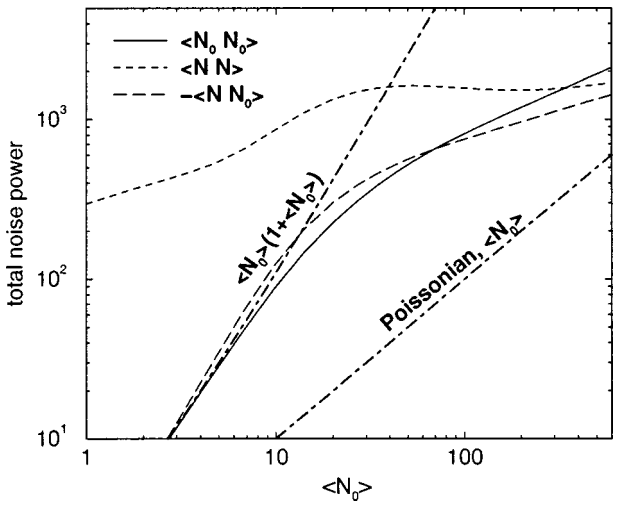

FIG. 6. Power noise spectra, as functions of the polariton population $\bar{N}_0$, for $T=6$ K, $\tau_0=10$ ps, and a 2×2 μm post structure.

$$S=\delta B_0+c\frac{\bar{B}_0\dot\phi}{\Gamma_0}=\frac{\delta N_0}{2\bar{B}_0}+c\frac{\bar{B}_0\dot\phi}{\Gamma_0},\tag{27}$$

where $c\ll1$ is an arbitrary real number. In practice, the weak mixing beam can be generated by simply delaying a weakly reflected beam, and the whole operator generated in the Mach-Zender interferometer configuration. The power spectrum of S is calculated inserting Eq. (21) in the above equation:

$$P_{S^\dagger S}(\omega)\sim\frac{1}{4\bar{N}_0}\left(1+\frac{3\mathcal{W}}{2\Gamma_0}\bar{N}_0|X|^4c\right)P_{\delta N_0^\dagger\delta N_0}(\omega).\tag{28}$$

Then, choosing $c\sim-3\mathcal{W}/2\Gamma_0\bar{N}_0|X|^4$, perfect squeezing is achieved (neglecting the background phase-diffusion processes, giving a small contribution $\propto c^2$ only). It is not obvious how to observe this strong internal squeezing, as internal polariton detection would be required. The result has, however, a deep physical significance. Far above threshold, the frequency carries all the information on the polariton number fluctuations. This information is retrieved through the mixing process of Eq. (27), which generates a noiseless polariton state in the microcavity.

Alternatively to the internal detection, we may consider the statistical properties of polaritons extracted from the microcavity. For example, polaritons could tunnel to an external exciton reservoir. In this paper, we consider only tunneling through the mirrors to external photons, which is also a reservoir of continuum modes. Using the input-output formalism of Gardiner and Collett [27], we may write the external field $R(t)$ as

$$R(t)=\sqrt{\Gamma_e}B_0(t)-F_e(t).\tag{29}$$

Here Γ_e is the input-output coupling strength, and F_e is an external white-noise source. In the micropost case, where most of the polariton loss is due to radiative recombination, we may set $\Gamma_e=\Gamma_0$. We also have $F_e(t)=F_{\Gamma_0}/\sqrt{\Gamma_e}$. When

$\bar{N}_0 \gg 1$, also $R(t)$ has small fluctuations around its average value $\bar{R} = \sqrt{\Gamma_0}\bar{B}_0$ with $R = (\bar{R} + \delta R)e^{-i\psi}$, where δR and ψ are Hermitian number fluctuation and phase operators, respectively. We then have

$$\delta R = \sqrt{\Gamma_0}\delta B_0 - \frac{1}{2}(F_e e^{i\phi} + e^{i\phi}F_e^\dagger),$$

$$\psi = \phi + \frac{1}{2i\bar{R}}(F_e e^{i\phi} - e^{i\phi}F_e^\dagger). \tag{30}$$

A mixed external operator S_e may be introduced for the internal field:

$$S_e = \delta R + c\frac{\bar{R}\dot{\psi}}{\Gamma_0}. \tag{31}$$

Transforming to the frequency space, and using Eq. (21), we have

$$S_e(\omega) = \frac{\sqrt{\Gamma_0}}{2\bar{B}_0}[1 + (\xi_0 + \xi_1)c]\delta N_0 + c\bar{B}_0\sqrt{\Gamma_0}\xi_2\delta N$$

$$+ i\frac{c}{2\sqrt{\Gamma_0}}[F_{B_0} - F_{B_0}^\dagger + F_{\Gamma_0} - F_{\Gamma_0}^\dagger] - \frac{1}{2}[F_e + F_e^\dagger].$$

Here we introduced the notation $\xi_0 = (3\mathcal{W}\bar{N}_0|X|^4)/(2\Gamma_0)$, $\xi_1 = \epsilon(N)/\Gamma_0$, and $\xi_2 = (d\epsilon/d\bar{N})/\Gamma_0$. From this expression the noise power is easily calculated. Far above threshold, $\xi_0 \gg \xi_1, \xi_2$, and also $\eta \gg \eta', \Gamma_0$. Considering $\omega < \Gamma_0$ within the cavity bandwidth, we obtain

$$P_{S_e^\dagger S_e} \sim (1 + \xi_0 c)^2 - (1 + \xi_0 c) + \frac{1}{2}(1 + c^2).$$

Using also $\xi_0 \gg 1/2$ we obtain a minimum noise power of 1/4, at $c = -1/(2\xi_0)$. This is a moderate 3 dB squeezing with respect to the standard quantum limit (SQL) of 1/2. This result has a simple physical interpretation. Polariton number fluctuations result equally well from the radiative loss process, and from pump fluctuations, which we considered to be Poissonian (incoherent pumping), in Eq. (16). The fluctuations originating from the radiative loss process cancel outside the cavity, within the cavity bandwidth, by beating with the external noise source F_e [26]. Usually, we are thus left with pump noise only within the cavity bandwidth. Clearly, the phase fluctuations far above threshold in the micropost system carry the information of the polariton number fluctuations. If, through the mixing process represented in Eq. (31), we cancel completely the number noise fluctuation, which corresponds to using $c = -1/\xi_0$, we are left with the standard noise from F_e. The best we can do is therefore to use half the latter value of c: half of the fluctuations from the radiative decay will be canceled in the beating with F_e, and half of the pump fluctuations will still be left. This finally makes 1/4 of noise from the radiative recombination process, and 1/4 of the pump noise, adding to a total noise power of 1/4.

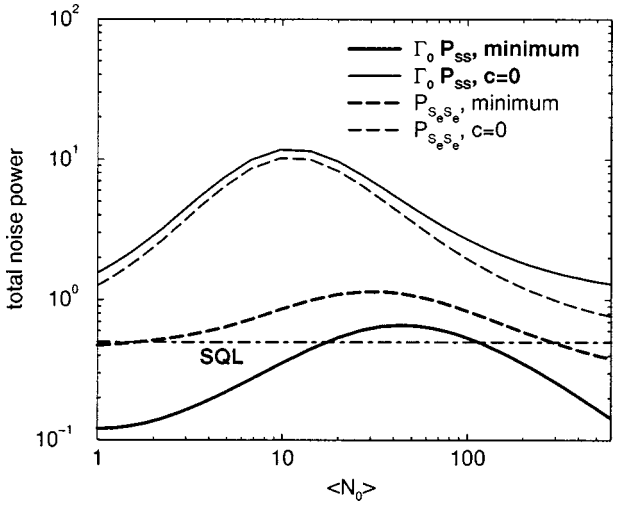

FIG. 7. Power noise at zero frequency for the mixed operator S and S_e of Eqs. (27) and (31), respectively, as functions of the polariton population $\bar{N}_0$, for $T = 6$ K, $\tau_0 = 10$ ps, and a 2×2 μm post structure.

In the GaAs structures considered in this paper the far-above-threshold condition is not reached, and we have therefore evaluated numerically both the internal and external optimal noise powers that can be obtained through the mixing process of Eqs. (27) and (31), respectively. Results are presented in Fig. 7. A suppression of the noise power is obtained both around threshold, and above it, for both the internal and external fields. The suppression is largest close to threshold. About 8 dB of internal polariton squeezing is observed at the largest $\bar{N}_0$, but barely 1 dB of squeezing is predicted for the external field squeezing at this point with respect to the SQL. Thus, external field squeezing is likely to be observed close to threshold only. Such an observation would be interesting, and prove the existence of strong phase modulation in the system. It is not self-phase modulation, which is dominant far above threshold only, as also numerically checked. Lasing in the far-above-threshold condition must be realized in real samples before these effects can be detected.

C. Emission linewidth

In stationary conditions, the spectral shape of emission is given by the following correlation function [22,25]:

$$I(\omega) = \int_{-\infty}^{\infty} d\tau\, e^{-i\omega\tau}\langle A^\dagger(\tau)A(0)\rangle. \tag{32}$$

Here $A(\tau)$ is the electromagnetic field amplitude at the detector position, outside the cavity. As the external vacuum field fluctuations do not contribute to the above expression, we may also substitute $B_0(\tau)$ for $A(\tau)$ in the above, apart from trivial delays.

Below threshold, the system behaves as a simple damped harmonic oscillator, and the calculation of the above average is straightforward using the quantum regression theorem [22]. We obtain a simple Lorentzian lineshape, of width γ

$=\Gamma_0-\bar{G}=\bar{R}_{sp}/\bar{N}_0$. When $\bar{N}_0 \ll 1$, $\gamma=\Gamma_0$, whereas above threshold, as $\bar{R}_{sp}$ becomes clamped and $\bar{N}_0$ increases linearly, a linewidth reduction of the Schawlow-Townes type is found. This is however only qualitative, as the above analysis cannot be applied beyond threshold, where the fluctuations δN become relevant. Far above threshold, the lineshape can be connected with the phase diffusion coefficient, [25] giving

$$I(\omega) \propto \int_0^\infty d\tau\, e^{-i\omega\tau} e^{-\langle [\phi(\tau)-\phi(0)]^2 \rangle}. \tag{33}$$

In calculating $\langle [\phi(\tau)-\phi(0)]^2 \rangle$, the imaginary noise sources in Eq. (21) decouple from the number fluctuations. We have two separate contributions. The first one originating from the noise terms in Eq. (21) is straightforward to calculate

$$\langle [\phi(\tau)-\phi(0)]^2 \rangle_{ST} = \frac{\bar{R}_{sp}}{2\bar{N}_0}\tau. \tag{34}$$

When inserted in Eq. (33), it gives an exponential decay in τ and a Lorentzian lineshape of width

$$\Delta\omega_{ST} = \frac{\bar{R}_{sp}}{\bar{N}_0}. \tag{35}$$

The calculation of the contribution from the number fluctuations to the linewidth is more involved, as these have colored spectrum and are correlated. The line shape can be calculated exactly using

$$\langle [\phi(\tau)-\phi(0)]^2 \rangle = \int_0^\tau dt_1\, dt_2 \langle \dot{\phi}(t_1)\dot{\phi}(t_2) \rangle,$$

inserting Eq. (21), passing to Fourier space, and using the solutions for $\delta N(\omega)$ and $\delta N_0(\omega)$ given in Eqs. (B1) in Appendix B. We first analyze different contributions separately, in the far above threshold limit, $\bar{N}_0 > \bar{N}$. We consider the two terms $(d\epsilon/d\bar{N})\delta N + \epsilon \delta N_0/2\bar{N}_0$ in Eq. (21). As well known from semiconductor laser theory, they produce an enhancement of the linewidth $\Delta\omega_{ST}$ in this regime. Using the Lorentzian line shapes of the noise sources, discussed in Sec. IV A, we find

$$\Delta\omega_{enh} = \frac{8\xi_2^2\Gamma_0^2\bar{R}_{sp}}{\eta^2}\bar{N}_0. \tag{36}$$

Here, $\xi_2=(d\epsilon/d\bar{N})/\Gamma_0$ was introduced before. In practice, $\xi_2 \sim 0.5|X_0|^2\mathcal{W}/\Gamma_0$. The enhancement factor is

$$\alpha^2 = \frac{\Delta\omega_{enh}}{\Delta\omega_{ST}} \sim \frac{8\xi_2^2\Gamma_0^2}{\eta^2}\bar{N}_0^2. \tag{37}$$

In the typical case of $D=2$ μm, at $T=6$ K, we have calculated microscopically $\alpha^2 \sim 10$. These are also typical values in semiconductor lasers.

Next, we calculate the contribution of the self-phase modulation term far above threshold. We find

$$\langle [\phi(\tau)-\phi(0)]^2 \rangle_{SPM} = \frac{\xi_0^2\Gamma_0}{\bar{N}_0}\left[\tau - \frac{1-e^{-\Gamma_0\tau}}{\Gamma_0}\right]. \tag{38}$$

Here $\xi_0=(3\mathcal{W}\bar{N}_0|X|^4)/(2\Gamma_0)$ was introduced before. When this correlation is inserted in the exponential of Eq. (33), a nonexponential decay is produced. We may identify two different regimes:

$$\langle [\phi(\tau)-\phi(0)]^2 \rangle_{SPM} \sim \begin{cases} \dfrac{\xi_0^2\Gamma_0^2}{2\bar{N}_0}\tau^2, & \Gamma_0\tau \ll 1, \\ \dfrac{\xi_0^2\Gamma_0}{\bar{N}_0}\tau, & \Gamma_0\tau \gg 1. \end{cases} \tag{39}$$

Clearly, simple exponential decay in Eq. (33) dominates when $\xi_0^2/\bar{N}_0 \sim \mathcal{W}^2\bar{N}_0/\Gamma_0^2 \ll 1$, otherwise, decay is of type $\exp(-\Delta\omega_G^2\tau^2)$. We thus have a Lorentzian or a Gaussian line shape respectively, of width

$$\Delta\omega_{SPM} = \begin{cases} \dfrac{\xi_0^2\Gamma_0}{\bar{N}_0}, & \dfrac{\xi_0^2}{\bar{N}_0} \ll 1, \\ \dfrac{\ln(2)\xi_0}{\sqrt{\bar{N}_0}}, & \dfrac{\xi_0^2}{\bar{N}_0} \gg 1. \end{cases} \tag{40}$$

As $\xi_0 \propto \bar{N}_0$, both linewidths *increase* with $\bar{N}_0$, and eventually dominate the Schawlow-Townes contribution, which instead decreases as $\bar{N}_0^{-1}$. This linewidth increase is as peculiar to this system as the self-phase modulation is. The relevant energy $\mathcal{W}$ is at the origin of both gain and of self-phase-modulation.

For the micropost with $D=2$ μm and $\Gamma_0=(10\text{ ps})^{-1}$, and $T=6$ K, we show in Fig. 8, the Schawlow-Townes linewidth, and the linearly increasing linewidth calculated from the self-phase modulation in Eq. (40). We did not include the linewidth enhancement, as the linearization procedure of the Langevin equation is not reliable around threshold ($\bar{N}_0 \sim 1$). An enhancement of about 10 should be smoothly introduced when $\bar{N}_0 \gg 1$. The calculation suggests that self-phase-modulation contribution is noticeable for $\bar{N}_0 > 80$. Even taking into account the linewidth enhancement α^2, the self-phase modulation contribution would be noticeable for $\bar{N}_0 > 200$. Therefore, we can optimistically expect that this linewidth enhancement will be eventually observed in these structures, before Rabi splitting collapse. The expected linewidth behavior as a function of emission intensity, i.e., first the Schawlow-Townes narrowing, then broadening, has been actually already observed in the nonlinear emission from Group-II–VI microcavities [30]. It is however premature to claim observation of the self-phase modulation effect in this system.

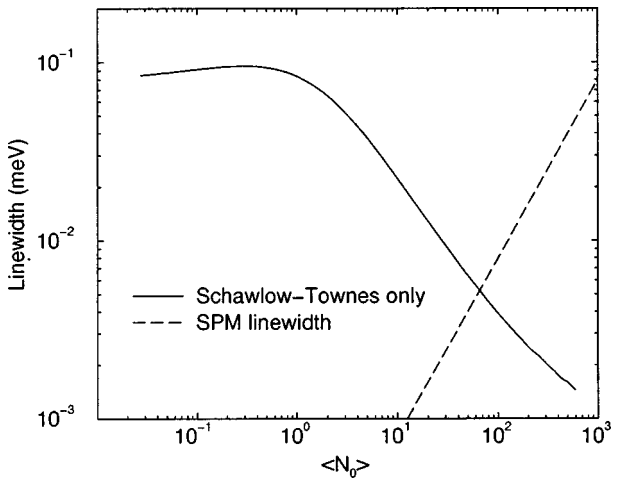

FIG. 8. Emission linewidth as a function of the polariton population, for $T=6$ K, $\tau_0=10$ ps, and a 2×2 μm post structure. The Schawlow-Townes linewidth and self-phase modulation linewidth are shown separately. The enhancement factor of Eq. (37) has not been included.

V. DISCUSSION AND CONCLUSIONS

The results of this paper are based on many assumptions, which we discuss in more detail here. Central to the model is the bosonic representation of the system, including the boson-boson interaction. The interaction originates in the exchange between the fermionic constituents of the excitons, and is thus an effect of the Pauli exclusion principle, as discussed in detail in Ref. [7]. Calculation of higher-order interaction terms between excitons (three-body interaction and so on) is cumbersome, and to the knowledge of the authors, it has never been addressed quantitatively. In this sense, the model presented here remains qualitative, and only a close comparison to experimental results provides a reliable estimate of its range of validity. Thus, successful fitting of scattering experiments up to densities of a few 10^9 cm^{-2} with this interacting boson model in Refs. [17,18] is a strong indication of its reliability in this range of densities.

Next, we discuss disorder effects of real samples. These are related to (static) fluctuations of the large barrier potential, which confines electrons and holes inside the QW. The disorder potential for the exciton has a typical amplitude $\sim E_B$, and correlation lengths of the order of a_B. This large amplitude is not directly observed in the optical properties of the QW (through inhomogeneous broadening), because of exciton delocalization. A characteristic length l may be introduced to characterize either the localization or diffusion length of the exciton motion. It amounts to a few a_B. The exciton-phonon and exciton-exciton scattering rates used in this paper are calculated for free, unperturbed, exciton motion. For thermalized excitons, this is still a reasonable assumption if the thermal wavelength $\lambda_{th}<l$. Thus, we expect exciton-exciton scattering to be gradually suppressed at low temperature, and in a sample dependent way, as the excitons gradually localize. After this point, localized excitons effectively behave as two-level atoms, and the bosonic description looses its meaning. Even in these extreme conditions, holding only at very low T, the polariton of a planar cavity is effectively delocalized, and showing bosonic properties. Indeed, hundreds of localized excitons are found within the wavelength of light, and even more so in a microcavity, where the cavity photon has an enhanced lateral wavelength [28]. The polariton becomes analogous to the superradiant state of N two-level atoms [29] and the bosonic assumption for the dynamics of the confined polariton is thus rather solid. This analogy also holds in the micropost considered in this paper. We remark that experiments aimed at directly showing the bosonic nature of polaritons produced positive results [17,18]. Moreover, these results were also successfully analyzed within the exciton-exciton scattering framework used in this paper, giving also evidence for the dominance of free excitons in the dynamics of the real samples already at $T=5$ K. As interface quality in Group-II-VI materials is comparable or presumably better than in Group-III–V based structures, we expect the free exciton picture to hold to even lower k_BT/E_B. The larger Rabi splittings of these materials makes them more advantageous than Group-III–V materials as explained in Sec. III. It is thus possible that in a recent observation of emission nonlinearities in Group-II–VI planar microcavities in Ref. [30], gain related to exciton-exciton scattering is involved. Possibly, lasing threshold has already been reached.

We finally discuss analogies and differences between the polariton, the bosonic atom, and conventional semiconductor lasers. Most proposed schemes for bosonic atom lasers share the same basic ingredients: stimulated emission from a cold atomic reservoir, or eventually from a few discrete levels, into the lowest mode of an atomic trap [4]. Different gain mechanisms have been proposed, many of which include atomic collisions [31]. The problem of extraction of atoms from the highly populated trapped mode has also been addressed [32], while it is open in the polariton case. Striking differences are found in the lifetimes or losses—seconds for trapped atoms, but only tens of ps for polaritons—and in the trapping energies—tens of nK for atomic traps but tens of K in the polariton case. The long lifetimes favor the realization of stimulated emission in the atomic system, making even tiny gains sufficient. The small trapping energies instead call for ultracold reservoirs, and are the main technological obstacle to the realization of the atomic laser, which has been already overcome with the use of evaporative cooling [33]. The similarities of a micropost polariton laser with a vertical cavity semiconductor lasers (VCSEL) is instead only structural. In these latter systems, stimulated emission of the confined photon modes is driven by fermionic population inversion. This is conceptually different from the stimulated emission of a confined polariton, which has an exciton content $\sim 90\%$ for $D=2$ μm, and is thus a composite boson. Moreover, the excitation density at threshold for the VCSEL is at least one order of magnitude larger. Finally, in the polariton laser, in complete analogy to the bosonic atom laser and in contrast to conventional photon lasers, excitation of the lasing mode is not *created* by the gain mechanism, but rather *transferred* from a reservoir.

In conclusion, we predicted and analyzed stimulated emission of reservoir excitons into the lowest confined polariton mode of a semiconductor microcavity post structure.

In typical GaAs based structures, exciton-exciton scattering provides sufficient gain to overcome large losses, up to $(10\ \mathrm{ps})^{-1}$, at an exciton density below that where the Rabi splitting collapses. We studied the threshold behavior of the stimulated emission for different post sizes, losses, and lattice temperatures. We put into evidence heating effects in the exciton reservoir, and the existence of an optimal lattice temperature. Statistics of the polariton becomes Poissonian far above threshold. Relevant self-phase modulation enhances phase noise, and eventually results into a net increase of the emission linewidth. We showed that strong correlation between frequency and number noise can be used to produce a number-squeezed polariton state. We discussed effects of interface disorder, advantages of Group-II–VI based structures, and conceptual differences with a conventional laser system. We remark that these micropost lasers are also technologically appealing as ultralow threshold sources of coherent light.

APPENDIX A: DERIVATION OF PERTURBATIVE LANGEVIN EQUATIONS FOR EXCITON-EXCITON SCATTERING

We consider the interaction of a confined polariton mode with the exciton reservoir. Confinement lifts momentum conservation. However, a quasiconservation over a momentum width of π/D is still valid. As the exciton distribution spans a much larger phase space, we may ignore such details. Moreover, the polariton mode has $|\mathbf{k}_p|=\pi/D\sim 0$ compared to those larger momentums. The relevant interaction Hamiltonian reads

$$\mathcal{H}=\frac{\hbar\mathcal{W}}{4}\sum_{\mathbf{k},\mathbf{k}',\mathbf{q}} X^*_{\mathbf{k}+\mathbf{q}}X^*_{\mathbf{k}'-\mathbf{q}}X_{\mathbf{k}'}X_{\mathbf{k}}b^\dagger_{\mathbf{k}+\mathbf{q}}b^\dagger_{\mathbf{k}'-\mathbf{q}}b_{\mathbf{k}'}b_{\mathbf{k}}, \tag{A1}$$

where $b_{\mathbf{q}}$ are the exciton or polariton destruction operators, $X_{\mathbf{k}}$ is the Hopfield coefficient (which is 1 for excitons having $k\neq 0$) and $\hbar\mathcal{W}\sim 6E_Ba_B^2/S$ [7]. We introduce the slowly varying operators, $B_{\mathbf{k}}(t)=e^{i\omega_{\mathbf{k}}t}b_{\mathbf{k}}(t)$, where $\hbar\omega_{\mathbf{k}}$ is the exciton energy at $\mathbf{k}$. The Heisenberg equations read

$$\begin{aligned}\dot{B}_{\mathbf{k}}(t)&=-\frac{i}{\hbar}[\mathcal{H}(t),B_{\mathbf{k}}(t)]\\&=-\frac{i\mathcal{W}}{2}\sum_{\mathbf{k},\mathbf{q}} X^*_{\mathbf{k}+\mathbf{q}}X^*_{\mathbf{k}'-\mathbf{q}}X_{\mathbf{k}'}X_{\mathbf{k}}B^\dagger_{\mathbf{k}'+\mathbf{q}}B_{\mathbf{k}'}B_{\mathbf{k}+\mathbf{q}}\\&\quad\times e^{i\Delta\omega_{\mathbf{k},\mathbf{k}',\mathbf{q}}t}.\end{aligned} \tag{A2}$$

Here $\Delta\omega_{\mathbf{k},\mathbf{k}',\mathbf{q}t}=\omega_{\mathbf{k}}+\omega_{\mathbf{k}'}-\omega_{\mathbf{k}+\mathbf{q}}-\omega_{\mathbf{k}'-\mathbf{q}}$. We are mainly interested in calculating the evolution of B_0. The drift terms are calculated taking statistical averages of the Heisenberg equation, and expanding them up to second order within a Markov approximation. The perturbative Langevin equations are finally written by substituting the remainder fluctuation sources (with zero average) with the appropriate sources having a white-noise spectrum [22]. In the averaged drift terms, first-order terms in the interaction Hamiltonian are usually neglected as they do not produce any scattering. However, they produce energy shifts. These are simple mean-field terms. We want to include these shifts in the Langevin equations, as they entail a coupling between amplitude and phase, and a characteristic broadening effect. Let us examine the averaged first-order terms for $\dot{B}_0$ in detail. Using the assumption that the excitons are a thermal reservoir, we have

$$\begin{aligned}\left\langle\frac{-i}{\hbar}[\mathcal{H}(t),B_0(t)]\right\rangle&=-i\frac{\mathcal{W}|X_0|^2}{2}\langle B_0(t)\rangle\sum_{\mathbf{k}\neq 0}\langle N_{\mathbf{k}}\rangle\\&\quad-i\frac{\mathcal{W}|X_0|^4}{2}\langle B_0^\dagger B_0^2\rangle.\end{aligned} \tag{A3}$$

The first term is the energy shift of the polariton level due to population in the exciton reservoir. The other one originates from the interaction term $\mathcal{W}|X_0|^4B_0^\dagger B_0^\dagger B_0^2/4$, and is discussed at length in Sec. IV.

In order to derive of the second-order terms in the Markov approximation, the reservoir coherence variables $\langle B^\dagger_{\mathbf{k}'+\mathbf{q}}B_{\mathbf{k}'}B_{\mathbf{q}}\rangle$ are adiabatically eliminated, just as in the conventional laser theory. It can be shown that this adiabatic elimination is actually valid precisely when exciton spectrum renormalization is negligible, as discussed before in Sec. IV [34]. The resulting averaged drift terms to second order in the interaction $\mathcal{W}$ are given by [22]

$$\langle D_{B_0}(t)\rangle=-\frac{1}{\hbar^2}\int_0^\infty d\tau\langle[H(t+\tau),[H(t),B_0(t)]]\rangle.$$

The commutator is given by

$$\sum_{\mathbf{k}_1,\mathbf{q}_1,\mathbf{k}_2,\mathbf{q}_2} e^{-i\Delta\omega\tau}[B^\dagger_{\mathbf{q}_1}B^\dagger_{\mathbf{k}_1-\mathbf{q}_1}B_{\mathbf{k}_1},B^\dagger_{\mathbf{k}_2}B_{\mathbf{k}_2-\mathbf{q}_2}B_{\mathbf{q}_2}],$$

where $\Delta\omega=\omega_{\mathbf{k}}+\omega_0-\omega_{\mathbf{q}}-\omega_{\mathbf{k}-\mathbf{q}}$, and in the Markov approximation (where the slowly varying operators are constant during the ''collision times''), using bosonic commutation relations we find

$$\begin{aligned}\langle D_{B_0}(t)\rangle&=\frac{-i\mathcal{W}^2|X_0|^2}{2}\sum_{\mathbf{k},\mathbf{q}}\frac{1}{\Delta\omega-i\epsilon}\\&\quad\times(N_{\mathbf{q}}N_{\mathbf{k}-\mathbf{q}}-N_{\mathbf{k}}-2N_{\mathbf{k}}N_{\mathbf{k}-\mathbf{q}})\langle B_0(t)\rangle.\end{aligned} \tag{A4}$$

Here $\epsilon\to 0^+$ is a regularization parameter. In this equation we also have $\mathbf{k},\mathbf{q},\mathbf{k}-\mathbf{q}\neq 0$. From the rate equations for the population

$$\dot{N}_{\mathbf{k}} = \pi \mathcal{W}^2 |X_0|^2 \sum_{\mathbf{k},\mathbf{q}} \delta(\Delta\omega)[N_{\mathbf{k}-\mathbf{q}} N_{\mathbf{q}}(1+N_{\mathbf{k}})(1+N_0) - (1+N_{\mathbf{k}-\mathbf{q}})(1+N_{\mathbf{q}})N_{\mathbf{k}} N_0]$$

$$= \pi \mathcal{W}^2 |X_0|^2 \sum_{\mathbf{k},\mathbf{q}} \delta(\Delta\omega)[N_{\mathbf{k}-\mathbf{q}} N_{\mathbf{q}} - N_{\mathbf{k}} - 2N_{\mathbf{k}} N_{\mathbf{k}-\mathbf{q}}]N_0 + \pi \mathcal{W}^2 |X_0|^2 \sum_{\mathbf{k},\mathbf{q}} \delta(\Delta\omega) N_{\mathbf{k}-\mathbf{q}} N_{\mathbf{q}}(1+N_{\mathbf{k}}).$$

Thus, the real part of Eq. (A4), the net gain for the polariton, is just half of the net gain calculated in the rate equation for the population $N_{\mathbf{k}}$, as it should be for bosons. Concerning the imaginary part of Eq. (A4), it has also been included in the Langevin Eq. (8) together with the first-order term from Eq. (A3), as the $\epsilon(N)$ term. We note that the Kramers-Krönig relation trivially hold for the real and imaginary parts of Eq. (A4), with the frequency ω_0 as the frequency variable, because of its functional form. In the structures considered, the second-order shifts are much smaller than the first-order ones.

The noise terms are easily determined from the Einstein relation between the diffusion term $\langle D_{B_0^\dagger B_0}\rangle$, and the drift terms of $N_0 = B_0^\dagger B_0$. We thus find

$$\langle D_{B_0^\dagger B_0}\rangle = -\frac{2}{\hbar^2}\int_0^\infty d\tau \langle [H(t+\tau), B_0^\dagger(t+\tau)][H(t), B_0(t)]\rangle.$$

The expectation value is

$$\sum_{\mathbf{k}_1,\mathbf{q}_1,\mathbf{k}_2,\mathbf{q}_2} e^{-i\Delta\omega\tau}\langle B^\dagger_{\mathbf{q}_1} B^\dagger_{\mathbf{k}_1-\mathbf{q}_1} B_{\mathbf{k}_1} B^\dagger_{\mathbf{k}_2} B_{\mathbf{k}_2-\mathbf{q}_2} B_{\mathbf{q}_2}\rangle,$$

i.e., just one side of the previous commutator, thus giving

$$\langle D_{B_0^\dagger B_0}\rangle = \pi \mathcal{W}^2 |X_0|^2 \sum_{\mathbf{k},\mathbf{q}} \delta(\Delta\omega) N_{\mathbf{k}-\mathbf{q}} N_{\mathbf{q}}(1+N_{\mathbf{k}}) = \bar{R}_{sp}.$$

APPENDIX B: SOLUTION OF THE LANGEVIN EQUATIONS

The solution of the Langevin Eqs. (24) in frequency space reads:

$$\tilde{\delta}N_0(\omega) = \frac{i\omega+\Gamma+\eta+\eta'}{\Delta}[\tilde{F}_{N_0}+\tilde{F}'_{\Gamma_0}] + \frac{\eta}{\Delta}[\tilde{F}_\Gamma+\tilde{F}_p+\tilde{F}_N],$$

$$\tilde{\delta}N(\omega) = \frac{\Gamma_0-\bar{G}+i\omega}{\Delta}[\tilde{F}_\Gamma+\tilde{F}_p+\tilde{F}_N] - \frac{\bar{G}}{\Delta}[\tilde{F}_{N_0}+\tilde{F}'_{\Gamma_0}], \tag{B1}$$

with

$$\Delta = (\Gamma_0-\bar{G}+i\omega)(i\omega+\Gamma+\eta+\eta')+\bar{G}\eta. \tag{B2}$$

The power spectra are calculated from these solutions using the definition of the noise sources Eqs. (12)–(19):

$$\frac{1}{2}P_{\delta N_0^\dagger \delta N_0} = \frac{\omega^2+(\Gamma+\eta+\eta')^2}{|\Delta|^2}[D_{N_0N_0}+\Gamma_0\bar{N}_0] + \frac{\eta^2}{|\Delta|^2}[\Gamma\bar{N}+P+D_{N_0N_0}] - 2\,\frac{\eta(\Gamma+\eta+\eta')}{|\Delta|^2}D_{N_0N_0}, \tag{B3}$$

$$\frac{1}{2}P_{\delta N^\dagger \delta N} = \frac{\bar{G}^2}{|\Delta|^2}[D_{N_0N_0}+\Gamma_0\bar{N}_0] + \frac{\omega^2+(\Gamma_0-\bar{G})^2}{|\Delta|^2}\times[\Gamma\bar{N}+P+D_{N_0N_0}] - 2\,\frac{(\Gamma_0-\bar{G})\bar{G}}{|\Delta|^2}D_{N_0N_0}, \tag{B4}$$

$$\frac{1}{4}P_{\delta N^\dagger \delta N_0+\delta N_0^\dagger \delta N} = \frac{(\Gamma+\eta+\eta')\bar{G}}{|\Delta|^2}[D_{N_0N_0}+\Gamma_0\bar{N}_0] + \frac{\eta(\Gamma_0-\bar{G})}{|\Delta|^2}[\Gamma\bar{N}+P+D_{N_0N_0}] - \frac{\omega^2+(\Gamma_0-\bar{G})(\Gamma+\eta+\eta')-\eta\bar{G}}{|\Delta|^2}\times D_{N_0N_0}. \tag{B5}$$

Here $D_{N_0N_0} = (\bar{R}_{sp}-\bar{G})\bar{N}_0 + \bar{R}_{sp}(\bar{N}_0+1)$ is the population drift coefficient.

[1] C. Weisbuch, M. Nishioka, A. Ishikawa, and Y. Arakawa, Phys. Rev. Lett. **69**, 3314 (1992).
[2] For a review, Y. Yamamoto, F. Tassone, and H. Cao, *Semiconductor Cavity Quantum Electrodynamics*, Springer Tracts in Modern Physics Vol. 169 (Springer-Verlag, Heidelberg, 2000).
[3] A. Imamoglu, R. J. Ram, S. Pau, and Y. Yamamoto, Phys. Rev. A **53**, 4250 (1996).
[4] H. M. Wiseman and M. J. Collet, Phys. Lett. A **201**, 246 (1995); R. J. C. Spreeuw, T. Pfau, U. Janicke, and M. Wilkens, Europhys. Lett. **32**, 469 (1995).
[5] S. Pau, H. Cao, J. Jacobson, G. Bjork, Y. Yamamoto, and A. Imamoglu, Phys. Rev. A **54**, R1789 (1996).
[6] F. Tassone, C. Piermarocchi, V. Savona, A. Quattropani, and P. Schwendimann, Phys. Rev. B **56**, 7554 (1997).
[7] F. Tassone and Y. Yamamoto, Phys. Rev. B **59**, 10 830 (1999).
[8] R. Houdre *et al.*, Phys. Rev. B **52**, 7810 (1995).
[9] J. K. Rhee, D. Citrin, T. Norris, Y. Arakawa, and M. Nishioka, Solid State Commun. **97**, 941 (1996).
[10] F. Jahnke *et al.*, Phys. Rev. Lett. **77**, 5257 (1996).
[11] L. Schultheis, A. Honold, J. Kuhl, K. Kohler, and C. W. Tu, Phys. Rev. B **34**, 9027 (1986).
[12] C. Piermarocchi, F. Tassone, V. Savona, A. Quattropani, and P. Schwendimann, Phys. Rev. B **53**, 15 834 (1996).
[13] S. Pau, G. Bjork, J. Jacobson, H. Cao, and Y. Yamamoto, Phys. Rev. B **51**, 7090 (1995).
[14] C. Ciuti, V. Savona, C. Piermarocchi, A. Quattropani, and P. Schwendimann, Phys. Rev. B **58**, 7926 (1998).
[15] A. Honold, L. Schultheis, J. Kuhl, and C. W. Tu, Phys. Rev. B **40**, 6442 (1989).
[16] B. Deveaud, F. Clerot, N. Roy, K. Satzke, B. Sermage, and D. S. Katzer, Phys. Rev. Lett. **67**, 2355 (1991).
[17] F. Tassone, R. Huang, and Y. Yamamoto, e-print cond-mat/9808157 (unpublished).
[18] R. Huang, F. Tassone, and Y. Yamamoto, Phys. Rev. B **61**, R7854 (2000).
[19] V. Savona, F. Tassone, C. Piermarocchi, A. Quattropani, and P. Schwendimann, Phys. Rev. B **53**, 13 051 (1996).
[20] L. C. Andreani, F. Tassone, and F. Bassani, Solid State Commun. **77**, 641 (1991).
[21] D. S. Citrin, Phys. Rev. B **47**, 3832 (1995).
[22] W. H. Louisell, *Quantum Statistical Properties of Radiation* (Wiley, New York, 1973).
[23] N. N. Bogolyubov, V. V. Tolmachev, and D. V Shirkov, *A New Method in the Theory of Superconductivity* (New York, Consultants Bureau, 1959).
[24] M. Kitagawa and Y. Yamamoto, Phys. Rev. A **34**, 3974 (1986); K. Watanabe, Y. Ishida, Y. Yamamoto, H. A. Haus, and Y. Lai, *ibid.* **42**, 5667 (1990).
[25] M. Sargent, M. O. Scully, and W. E. Lamb, *Laser Physics* (Addison-Wesley, Reading, MA, 1977).
[26] Y. Yamamoto, S. Machida, and O. Nilsson, Phys. Rev. A **34**, 4025 (1986).
[27] C. W. Gardiner and M. J. Collett, Phys. Rev. A **31**, 3761 (1985).
[28] G. Bjork, S. Pau, J. Jacobson, and Y. Yamamoto, Phys. Rev. B **50**, 17 336 (1994); F. de Martini, M. Marrocco, P. Mataloni, L. Crescentini, and R. Loudon, Phys. Rev. A **43**, 2480 (1991).
[29] See e.g., M. Gross and S. Haroche, Phys. Rep. **93**, 301 (1982).
[30] Le Si Dang, D. Heger, R. André, F. Boeuf, and R. Romenstein, Phys. Rev. Lett. **81**, 3920 (1998).
[31] A. M. Guzman, M. Moore, and P. Meystre, Phys. Rev. A **53**, 977 (1996).
[32] G. M. Moy and C. M. Savage, Phys. Rev. A **56**, R1087 (1997); J. J. Hope, *ibid.* **55**, 2531 (1997).
[33] M. H. Anderson, R. J. Ensher, M. R. Matthews, C. E. Wiemann, and E. A. Cornell, Science **269**, 198 (1995).
[34] F. Tassone (unpublished).